

A. T. Motta,¹ K. T. Erwin,¹ O. Delaire,¹ R. C. Birtcher,² Y. Chu,³
J. Maser,³ D. C. Mancini,³ and B. Lai³

Synchrotron Radiation Study of Second-Phase Particles and Alloying Elements in Zirconium Alloys

REFERENCE: Motta, A. T., Erwin, K. T., Delaire, O., Birtcher, R. C., Chu, Y., Maser, J., Mancini, D. C., and Lai, B., "Synchrotron Radiation Study of Second-Phase Particles and Alloying Elements in Zirconium Alloys," *Zirconium in the Nuclear Industry: Thirteenth International Symposium, ASTM STP 1423*, G. D. Moan and P. Rudling, Eds., ASTM International, West Conshohocken, PA, 2002, pp. 59–79.

ABSTRACT: We have conducted a study of second phase particles and matrix alloying element concentrations in zirconium alloys using synchrotron radiation from the Advanced Photon Source (APS) at Argonne National Laboratory. The high flux of synchrotron radiation delivered at the 2BM beamline, compared to conventional X-ray generators, enables the detection of very small precipitate volume fractions. We detected the standard C14 hcp Zr(Cr,Fe)₂ precipitates (the stable second phase in Zircaloy-4) in the bulk material at a cumulative annealing parameter as low as 10⁻²⁰ h, and we followed the kinetics of precipitation and growth as a function of the cumulative annealing parameter (CAP) in the range 10⁻²² (quench) to 10⁻¹⁶ h. In addition, the unique combination of spatial resolution and elemental sensitivity of the 2ID-D/E microbeam line at the Advanced Photon Source at Argonne (APS) allows study of the alloying element concentrations at ppm levels in an area as small as 0.2 × 0.3 μm. We used X-ray fluorescence induced by this sub-micron X-ray beam to determine the concentration of these alloying elements in the matrix as a function of alloy type and thermal history. We discuss these results and the potential of synchrotron radiation-based techniques for studying zirconium alloys.

KEYWORDS: synchrotron radiation, zirconium alloys, alloying elements

The microstructure of zirconium alloys, especially the precipitate morphology, size, and distribution, is strongly correlated with in-reactor properties such as the degree of waterside corrosion and hydriding during reactor exposure [1]. Different thermal processing conditions lead to different microstructures; for example, the precipitate size increases with the annealing parameter [2,3]. The structure and morphology of second phase precipitates in Zr alloys as well as the concentration and distribution of the transition elements Fe, Cr, and Ni present in the α-Zr matrix of Zr alloys have been linked to several in-reactor degradation processes. In particular, enhanced levels of Fe in the matrix have been shown to change the intrinsic diffusion coefficient of Zircaloy and to influence the nucleation of <c>-component loops, which can accelerate irradiation growth [4]. Also, the rates of waterside corrosion are

¹ Department of Mechanical and Nuclear Engineering, The Pennsylvania State University, University Park, PA 16802.

² Materials Science Division, Argonne National Laboratory, Argonne, IL 06043.

³ Advanced Photon Source, Argonne National Laboratory, Argonne, IL 06043.

strongly related to the average precipitate size and annealing parameter of the material [5]. Understanding these links mechanistically requires direct measurement of the structure and volume fraction of these precipitates in the bulk alloy for particular thermo-mechanical treatments and the measurement of the very low alloying element concentrations in the matrix. Thus, the characterization of the microstructure of zirconium alloys used in nuclear applications is an essential factor in understanding their in-reactor behavior. However, the volume fraction of these precipitates is sufficiently small as to preclude the use of standard methods of phase determination using conventional X-ray generators. The low concentrations of alloying elements are below the resolution limits of traditional techniques, such as energy dispersive X-ray spectroscopy in the transmission electron microscope (TEM).

Previous research on the characterization of precipitates in Zircaloy-4 and Zircaloy-2 by transmission electron microscopy (TEM) has identified the crystal structure and morphology of the main precipitate types [6]. However, to fully characterize the precipitate size distribution, it is necessary to perform extensive TEM examinations and observe enough precipitates to obtain good statistics. Even with such information, it is difficult to derive a true precipitate volume fraction from these measurements. In parallel, researchers have also attempted to measure the alloying element content in the zirconium matrix of these alloys. The solubility of the transition metals such as Fe in zirconium alloys, such as Zircalloys, is quite low (although not as low as that in pure zirconium) [7]. The difficulty in measuring the alloying element content lies in the fact that the techniques that have the spatial resolution to differentiate the matrix from the precipitates do not have the elemental sensitivity to detect the low levels of alloying elements found in the matrix.

Recently, a new synchrotron facility, the Advanced Photon Source at Argonne National Laboratory, has become available that can help address some of these questions. Among the advantages of using X-ray radiation from synchrotron machines are the very high flux (and brilliance), the high degree of collimation and energy tenability of the X-ray beams they deliver. The high X-ray fluxes available at APS allow the detection of alloying element concentrations at the ppm level by X-ray fluorescence, and also allow the detection of very small volume fractions of precipitates by X-ray diffraction. One particular beamline at APS, the SRI-CAT, has an additional feature that is very useful to this study. In this beam line a circular grating (zone plate) is capable of focusing the X-ray beam emitted by the undulator (X-ray producing device used in third generation synchrotrons) to a 0.2 μm spot while maintaining the high X-ray fluxes [8,9]. We used both of these research capabilities, and in this work we present the experimental results we obtained.

Experimental Methods

Table 1 gives the concentrations (and the elemental detection limits) of the different alloys examined in this work, as measured by hot vacuum extraction. Zircaloy-4 and Zircaloy-2 samples were obtained from the General Electric Corporation as plate material. Samples suitable for X-ray diffraction were cut from the plate with a low-speed diamond saw and mechanically polished on a mechanical milling machine using 15 mm SiC paper. ZIRLO was obtained from Westinghouse Electric Corporation in the form of tubing. This material underwent a sequence of cold-pilgering and annealing in the temperature range 853 to 873 K for about 4 h each time [10]. Flat sections measuring about $5 \times 10 \times 0.5$ mm were prepared for X-ray diffraction by cutting, mechanically grinding, and polishing.

The Zircaloy samples were annealed in a quartz tube filled with ultra-high purity Ar for 10 min at 1170 K to completely dissolve the precipitates and put the alloying elements back into solution in the matrix. After the heat treatment, the samples were quenched by breaking the quartz tube over a bucket of water. A small amount of discoloration in these samples

TABLE 1—Chemical analysis of various zirconium alloys performed by Luvak Inc. All values are expressed in weight percent.

Element	Zircaloy-2	Zircaloy-4	ZIRLO	Detection Limit
Aluminum	0.0061	0.0058	0.012	0.0005
Carbon	0.002	0.003	0.002	0.0010
Chromium	0.11	0.11	0.001	0.0005
Copper	0.0046	0.0020	0.0020	0.0005
Hafnium	<0.004	<0.004	<0.004	0.0040
Iron	0.14	0.24	0.10	0.0005
Manganese	<0.001	<0.001	<0.001	0.0010
Molybdenum	<0.001	<0.001	<0.001	0.0010
Nickel	0.063	0.0034	<0.001	0.0010
Niobium	1.23	0.0010
Nitrogen	0.003	0.002	0.005	0.0010
Oxygen	0.112	0.112	0.145	0.0010
Silicon	0.0097	0.0095	0.013	0.0010
Tin	1.55	1.64	1.08	0.0010
Titanium	0.0020	0.0012	0.0019	0.0010
Tungsten	<0.004	<0.004	<0.004	0.0040
Zirconium	Balance	Balance	Balance	

resulting from the heat treatment was removed by further mechanical polishing. After quenching, the samples were re-sealed into quartz tubes and annealed to various values of the Cumulative Annealing Parameter (CAP) [3], defined as:

$$CAP = \sum_i t_i \exp(-Q/RT_i) \quad (1)$$

where t_i is the time (hours) spent at temperature T_i (K) and $Q/R = 40\,000$ K. Table 2 shows the range of annealing parameters for the samples studied. The ZIRLO samples were examined in the as-received state.

The samples used in X-ray fluorescence experiments were standard TEM thin foils (about 100 nm thick in their thinnest region) prepared from strips of the alloys that were brought to different cumulative annealing parameters with the heat-treatment procedure described above. These foils were prepared by mechanically grinding the strips to a thickness of approximately 100 μm , punching out 3 mm diameter disks, then electropolishing in a solution of 670 mL methanol, 100 mL of butoxyethanol, and 130 mL HCl, at a temperature of -60°C and an electropolishing current of 20 mA. These samples were examined by transmission electron microscopy in a Philips CM-30 transmission electron microscope at Argonne National Laboratory and at a Hitachi FE 2000 at Penn State.

Synchrotron X-ray Diffraction

Bulk X-ray diffraction was performed at the 2-BM beamline at the SRI-CAT at the Advanced Photon Source at Argonne. Figure 1a shows the beamline setup and Fig. 1b shows the acquisition geometry. The storage ring emits synchrotron radiation of continuous wavelength called the white X-ray beam. The apertured white beam is reflected off a Cr mirror, which serves as a low pass filter with a high-energy cutoff of 20 keV. A double crystal Si (111) monochromator selects a monochromatic X-ray beam with a bandwidth of $\delta E/E \sim$

TABLE 2—*Annealing schedules and cumulative annealing parameter for alloys examined.*

Alloy	Sample Designation	Annealing Temperature (°C)	Annealing Time (h)	CAP (h)
Zircaloy-4	Mz4q	0	0	0—as quenched condition
Zircaloy-2	Mz2q			
Zircaloy-4	Mz4e20c	605	1	1.63×10^{-20}
Zircaloy-2	Mz2e20c			
Zircaloy-4	Mz4e19c	650	1	1.5×10^{-19}
Zircaloy-2	Mz2e19c			
Zircaloy-4	Mz4e18c	700	1	1.4×10^{-18}
Zircaloy-2	Mz2e18c			
Zircaloy-4	Mz4e17c	759	1	1.46×10^{-17}
Zircaloy-2	Mz2e17c			
Zircaloy-4	Mz4e16c	815	1	1.07×10^{-16}
Zircaloy-2	Mz2e16c			
Zircaloy-4	Mz4q	0	0	0—as quenched condition
Zircaloy-2	Mz2q			
Zircaloy-4	Mz4e19t	720	0.0312	1.1×10^{-19}
Zircaloy-2	Mz2e19tc			
Zircaloy-4	Mz4e18t	730	0.312	1.49×10^{-18}
Zircaloy-2	Mz2e18t			
Zircaloy-4	Mz4e17t	725	3.12	1.22×10^{-17}
Zircaloy-2	Mz2e17t			
Zircaloy-4	Mz4e16t	725	31.2	1.22×10^{-16}
Zircaloy-2	Mz2e16t			
Zircaloy-4	Mz463e18	755	0.5	6.31×10^{-18}
Zircaloy-2	Mz263e18			
Zircaloy-4	Mz465e19t	725	0.1667	6.53×10^{-19}
Zircaloy-2	Mz265e19t			

10^{-4} . The size of the incident beam onto the sample is defined by the sets of slits. The intensity of the incident beam is measured by an ion chamber and is used to normalize the diffracted intensity. The sample is mounted on a standard four-circle diffractometer, and the diffracted beam is measured by a NaI scintillation detector. The slits before the detector are used to reduce the unwanted background produced by the incident beam. The energy used was 13 keV ($\lambda = 0.95348$ nm). We examined ZIRLO, Zircaloy-2, and Zircaloy-4 in the as-quenched state and after successive annealing schedules as described in Table 2. The chi and phi angles were kept at 90 and 0°, respectively.

Micro X-Ray Fluorescence

We performed microfluorescence examinations of the alloys by using a micro-focused beam on the 2ID-D/E beamlines at APS and placing it on the regions of interest. The beam intensity profile was measured by recording the fluorescence from a Cr knife edge scanned through the beam. The beam was determined to be 0.24 μm wide (FWHM), corresponding to a 0.30 by 0.24 μm footprint on the sample. The geometry of acquisition is shown in Fig. 1c. We minimized the parasitic fluorescence peak Ar in surrounding air by placing a He-filled bag around the sample. We used the sample stage rastering capabilities to acquire concentration maps for the elements of interest. In order to maximize the precipitate-free regions throughout the depth sampled in the specimen (and also because of beam spreading associated with thick samples), we elected to use thin foils as prepared for conventional

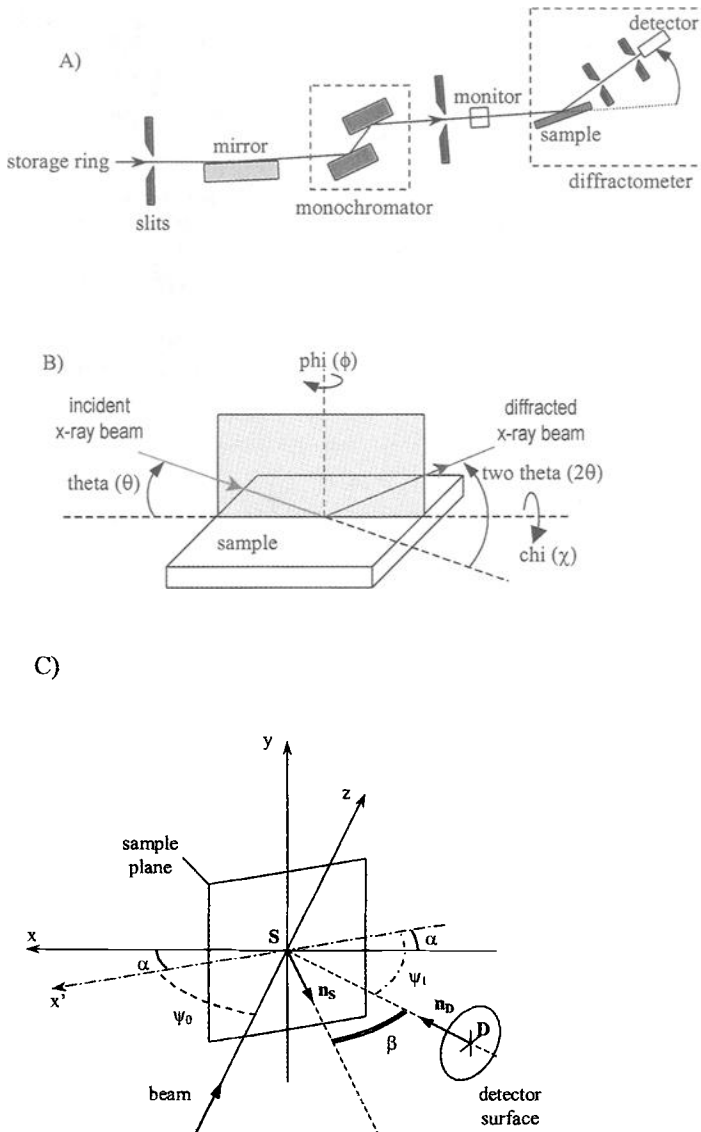


FIG. 1—(A) schematic view of the experimental setup at the 2-BM beamline at the Advanced Photon Source; (B) diffraction geometry used for the experiment; (C) acquisition geometry for the fluorescence experiments.

TEM examination. We followed a positioning procedure based on line scans running through the sample that allowed us to find the thinnest region. Staying in this very thin region, we then moved a small distance ($\sim 5 \mu\text{m}$) off the hole and took a 2D scan (typically $10 \times 10 \mu\text{m}$) to identify the location of any second phase particles, and of a suitable matrix spot from where to acquire a detailed fluorescence spectrum. Typical acquisition times for such spectra were on the order of 600 to 1500 s, which corresponds to a vastly larger number of

incident photons sampling the specimen than during a typical X-ray fluorescence experiment using a conventional X-ray tube source (even if run for many hours).

Results

The microstructures of the quenched and annealed materials were examined by TEM. Bright field micrographs of quenched Zircaloy-4, annealed Zircaloy-4, and annealed ZIRLO are shown in Fig. 2. The precipitate particles in Zircaloy-4 were indexed as the C14 hcp Laves Phase (MgZn_2 -type) commonly found in this alloy. The ZIRLO particles were indexed either bcc β -Nb or as Zr-Nb-Fe particles with an hcp structure, which has been recently indexed as having the same structure as the $\text{Zr}(\text{Cr,Fe})_2$ C14 Laves phase, in agreement with previous studies [11,12]. The quenched alloy showed no indication of second phase precipitation. The lath boundaries of the quenched alloy were examined with EDS and no alloying element enrichment detected.

X-Ray Diffraction

Figure 3 shows X-ray diffraction patterns obtained with synchrotron radiation (intensity vs. two-theta angle) for Zircaloy-4, Zircaloy-2 in the fully recrystallized state (10^{-16} h), and as-fabricated ZIRLO. We can index the peaks in the Zircaloy-4 spectrum as corresponding either to the α -Zr hcp phase or the C14 $\text{Zr}(\text{Cr,Fe})_2$ hcp Laves phase (MgZn_2 -type). The lattice parameters determined from the fit of the data correspond very well to the powder diffraction files for C14 hcp $\text{Zr}(\text{Cr,Fe})_2$ [13,14]. There are faint indications of $\text{Zr}_2(\text{Ni,Fe})$ peaks in Zircaloy-4, which could be related to the fact that at low densities Ni-based precipitates are found in Zircaloy-4, because the small impurity level amount of Ni ends up in these types of precipitates. In the Zircaloy-2 diffraction pattern, the same peaks are present but there are additional peaks that can be indexed as the body-centered tetragonal C16 $\text{Zr}_2(\text{Ni,Fe})$ phase [15]. For ZIRLO, in addition to α -Zr, β -Nb peaks with the bcc crystal structure are indexed in Fig. 3 [16]. The remaining peaks can be indexed as the C14 phase and can likely be identified with the Zr-Nb-Fe phase seen by Sabol et al. [12] and Erwin et al. [14]. The results in Fig. 3 demonstrate that the small volume fractions of second phase particles (<0.2 to 0.4%) can be detected and identified using synchrotron radiation. We note that it is possible to obtain some indication of these second phase peaks by conventional X-ray diffraction [14]. However, the counting times are much higher and the peaks much less well defined, so that much less information is available. We should also note that a few peaks in Fig. 3 are not indexed but have been empirically associated with a phase because they appear whenever the particular phase is present. The obvious candidates for additional phases present in Zircaloy-4, such as Zr_3Fe or cubic $\text{Zr}(\text{Cr,Fe})_2$, were tested, but found not to correspond to these peaks. The range of possible particles in Zircaloy-4 includes a variety of silicides and phosphides, and it is possible that the unindexed peaks originate from some of these phases.

We used synchrotron radiation to examine a series of Zircaloy-2 and Zircaloy-4 samples in the quenched state and after annealing up to $\text{CAP} = 10^{-16}$ h. The results of this examination are shown in Fig. 4. In the as-quenched material, both for Zircaloy-2 and Zircaloy-4, only the α -Zr peaks are observed. The Zr peaks are fairly broad, in agreement with the small grain size of the quenched microstructure. As the annealing parameter increases, the α -Zr peaks become sharper and new peaks appear that correspond to the second phase particles. For Zircaloy-4 these peaks correspond to the C14 $\text{Zr}(\text{Cr,Fe})_2$ phase. The second phase particle peaks are also initially broad ($\text{CAP} = 10^{-20}$ h) and of low intensity, indicating a small amount of second phase precipitated at that stage in the form of very fine particles, which are also



FIG. 2—Bright field transmission electron micrographs of (a) quenched Zircaloy-4, (b) fully annealed (10^{-16} h) Zircaloy-4 and (c) ZIRLO.

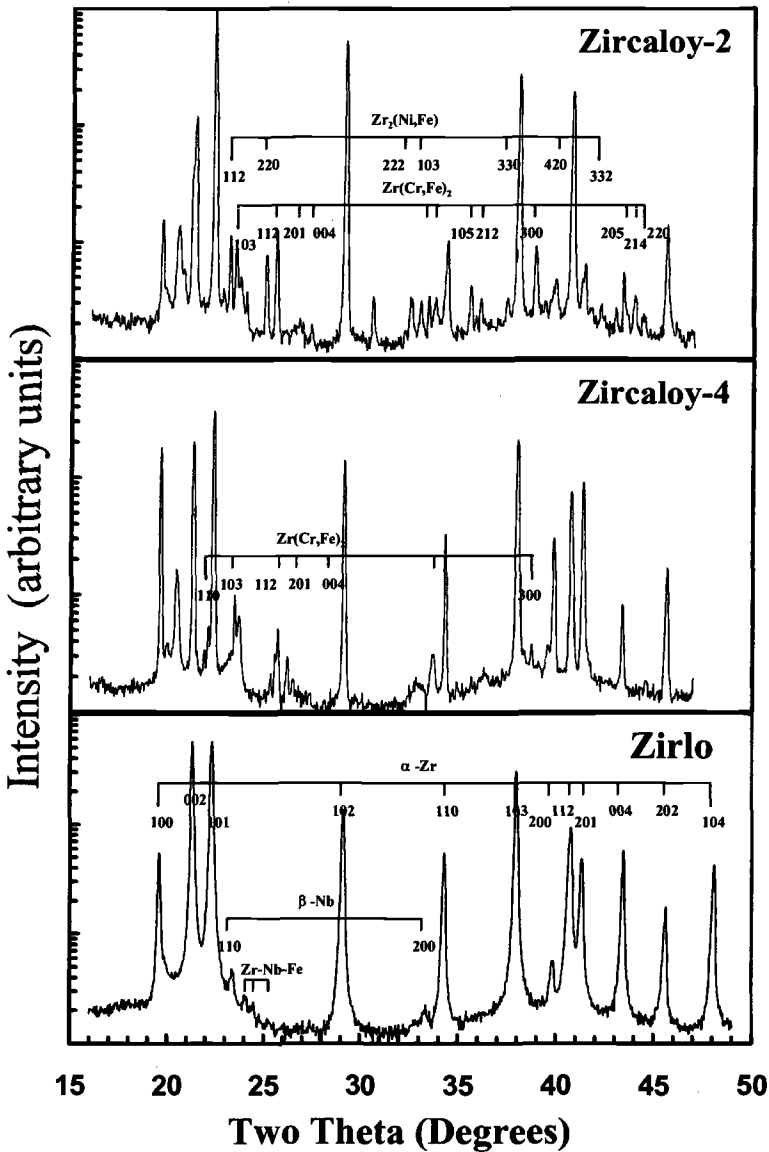


FIG. 3—Synchrotron radiation diffraction patterns for Zircaloy-2 and Zircaloy-4 (both annealed to 10^{-16} h), and ZIRLO (annealed to 10^{-18} h). The phases present are shown in the indexing bars in the figures.

possibly strained. As the CAP increases, the peaks sharpen and grow, indicating further precipitation out of solid solution and an increase in precipitate size. In Zircaloy-2 we see, in addition to the C14 phase peaks, the peaks corresponding to the $Zr_2(Ni,Fe)$ phase (indicated in Fig. 3), which also grow and sharpen.

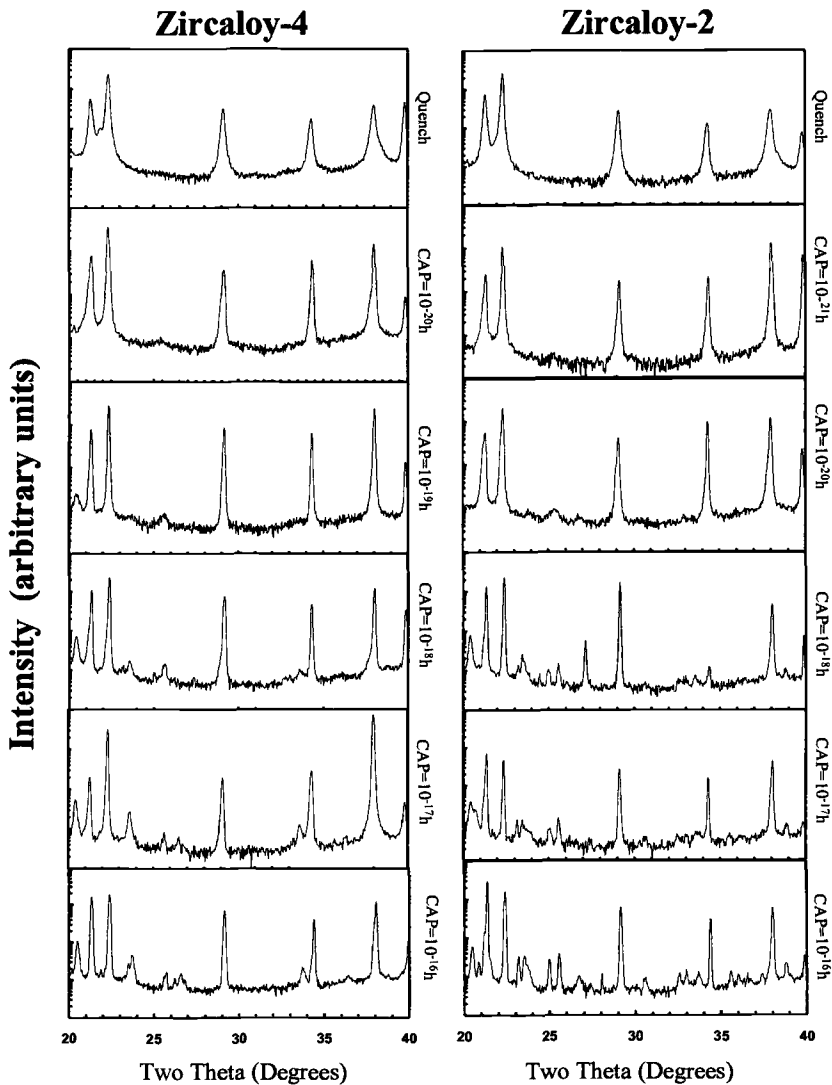


FIG. 4—Synchrotron radiation diffraction patterns for Zircaloy-4 and Zircaloy-2 as a function of annealing parameter.

X-Ray Microfluorescence

We used the micro beam-focused technique described under Experimental Methods to study the alloying element content in the zirconium matrix. Figure 5 shows the Fe, Cr, Zr, and Sn fluorescence scans of a thin foil region of Zircaloy-4, taken on a 10 by 10 μm grid and a step size of 0.4 μm . The 2D scan shows the position of intermetallic precipitates. We then placed the beam on the region in between the precipitates and performed a more detailed scan of the smaller region (typically 2 by 2 μm , with a 0.1 μm step size and an acquisition time of 5 s per point) to ensure that no large variations of Fe content exist within those

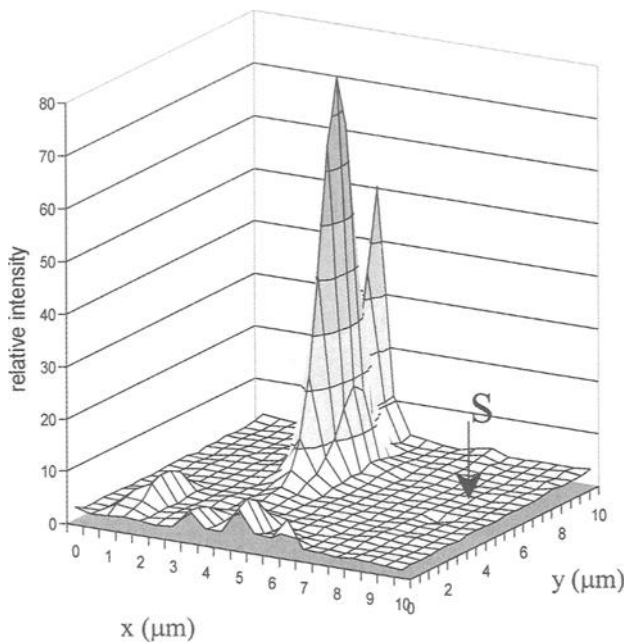


FIG. 5—2-D fluorescence scan of Fe, obtained from the examination of a TEM thin foil of Zircaloy-4 using a $0.25\ \mu\text{m}$ probe.

regions. We then positioned the beam in this lowest Fe region and acquired point spectra with long acquisition times, typically for 600 to 1500 s. These spectra serve as the basis for our quantitative analysis of the matrix composition in those samples.

Figure 6a shows several fluorescence spectra acquired from four standards: (i) a TEM foil of a quenched Zircaloy-4 sample, (ii) a bulk sample of nominally pure zirconium, (iii) bulk ultra pure zirconium (acquired from Chalk River Laboratories), and (iv) from TEM foil of quenched ZIRLO. In these samples, the concentrations should be close to those obtained from overall bulk measurements. We find that the Fe peaks are highest for Zircaloy-4, next for ZIRLO, then nominally pure Zr and lastly ultra pure Zr. The spectra are normalized by the Sn counts, since the Sn concentration is homogeneous in the Zr matrix in order to account for the different number of counts from sample to sample, resulting from different sample thicknesses. The value for the Fe content in the Zircaloy-4 matrix is higher than that found in nominally pure Zr, but considerably lower than that found in the quenched sample. One possible source of error in measuring alloy content in samples prepared by electropolishing could arise from the redeposition of alloying elements from the electropolishing solution onto the surface of the thin foil. To check for this possible error, we examined one recrystallized Zircaloy-4 sample that had undergone an ion milling procedure for 3 min after electropolishing; we observed no change in the concentrations before and after the ion milling, although the hole had been considerably enlarged. This indicates that this effect is not significant for our experiments. Figure 6b shows the same Zircaloy-4 quenched spectrum superimposed on the spectrum measured on a matrix spot of TEM foil made of fully recrystallized Zircaloy-4 ($\text{CAP} = 10^{-16}\ \text{h}$). The linear analysis gives an Fe concentration in the matrix of about 300 and 307 ppm for Cr.

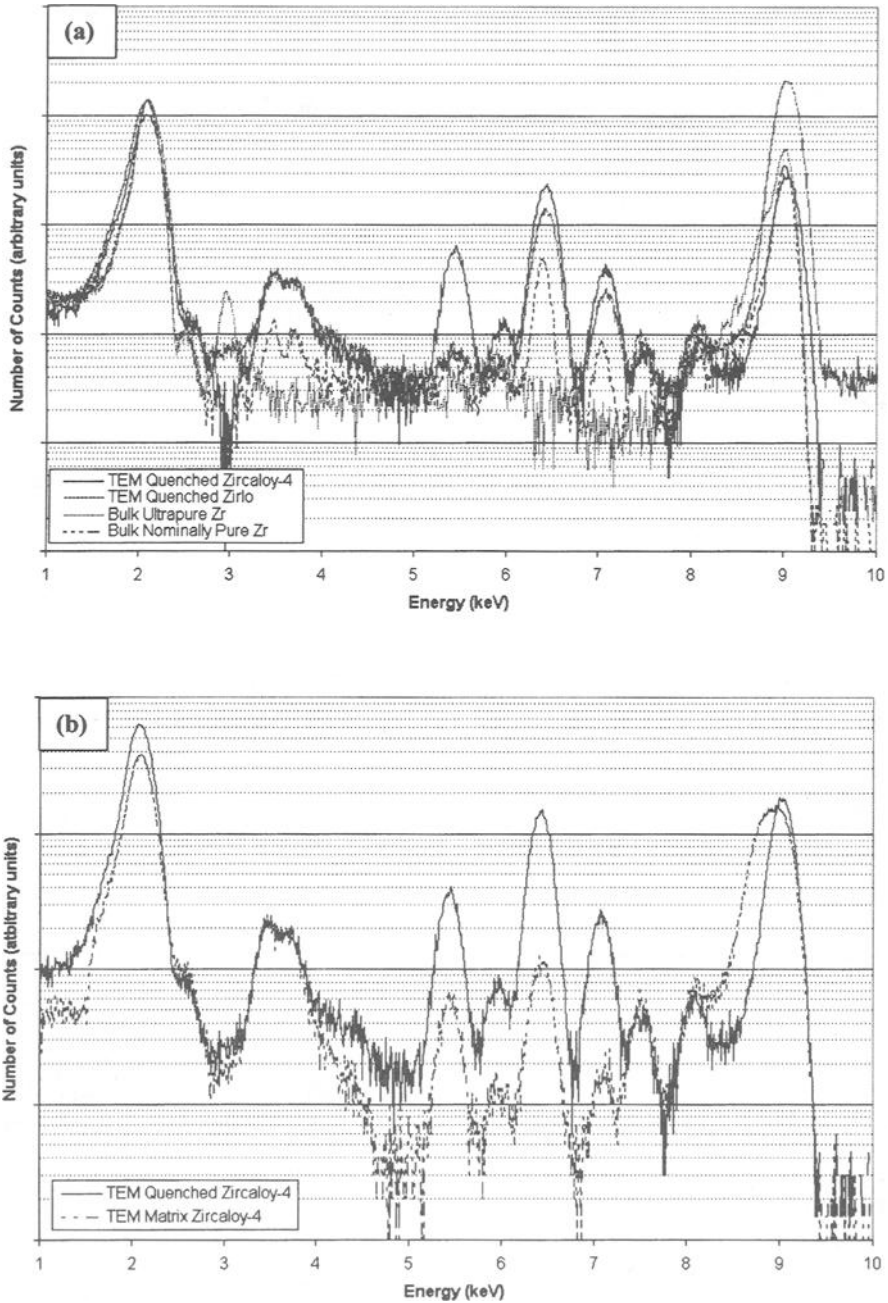


FIG. 6—Fluorescence spectra obtained from (a) quenched Zircaloy-4 TEM foil, quenched ZIRLO TEM foil, and ultra pure Zr (bulk sample) and (b) quenched Zircaloy-4 TEM foil and the matrix region in a TEM foil of annealed Zircaloy-4.

Table 3 shows a linear analysis of the composition of the alloys. The linear analysis is performed by taking the integrated ratio of the counts for a particular elemental peak and finding their ratio to a known standard (quenched Zircaloy-4 or quenched ZIRLO). The procedure is the following: by integration we find the total number of counts in the Zr peak and normalize that value to 106 counts. The same multiplication factor is then applied to the elemental peak; we can then compare the results obtained from other alloys. The linear analysis shows that if we assume that the alloying element concentrations to be the measured bulk values in the quenched alloys (e.g., assuming the Fe and Cr concentration in Zircaloy-4 to be 2400 and 1130 ppm (Table 1)), we can reproduce the concentrations in the other alloys (compare non-bolded values in Table 3 with those in Table 1). That is, the ratio of the alloying element concentrations is reproduced by the measurements. This gives confidence that the results are reliable. Table 3 also shows the results from the Monte Carlo program MSIM5D, discussed in the next section.

Analysis

X-Ray Diffraction Data

We have performed an initial analysis of our diffraction data by locating the peaks and manually fitting the expected phases for an optimized value of the lattice parameter. The measured values of the α -Zr matrix lattice parameter are $a = 0.3233$ nm and $c = 0.5159$ nm, which are similar to the literature values of 0.3232 and 0.5147 nm [17]. We also performed this analysis for the second phase particles. The chemistry of the second-phase particles (Fe/Cr or Fe/Ni ratios) affects their lattice parameter, as does the presence of size misfit stresses from precipitation of incoherent particles (for example, misfit strains could be as high as the yield stress divided by the elastic modulus for a precipitate that is harder than the matrix). Therefore, the lattice parameter of the particles in the alloy does not necessarily correspond to that in the literature values, and we fit the results to find the lattice parameter for the phases of interest.

The analysis yielded the values for the lattice parameters of the precipitates in the alloys shown in Table 4. These values are in good agreement with published values of the lattice

TABLE 3—*Calculated alloying element concentrations.*

	Calculated Concentrations			
	Quenched Zircaloy 4		MC Simulation	
	Fe K α (weight ppm)	Cr K α	Fe K α (weight ppm)	Cr K α
Quenched Zircaloy 4	2400	1130	2400	1130
Recrystallized Zircaloy 4 Matrix (10^{-16} h)	320	307	300	270
Quenched ZIRLO	1052	131	1070	10
As-fabricated ZIRLO Matrix	174	56	250	10
Nominally Pure Zr (Goodfellow Corporation)	390	112	310	10
Ultra-Pure Zr (Chalk River National Laboratories)	24	65	10	10

TABLE 4—*Lattice parameters of second phase precipitates (nm).*

	Zr(Cr,Fe) ₂ (hcp C14)	Zr ₂ (Ni,Fe) (bct C16)	Zr-Nb-Fe (hcp C14)
Zircaloy-2	$a = 0.500$ $c = 0.820$	$a = 0.648$ $c = 0.526$	x
Zircaloy-4	$a = 0.501$ $c = 0.821$	x	x
ZIRLO	x	x	$a = 0.53$ $c = 0.875$

parameters for these crystal structures from TEM studies [6]. For the Zr₂(Ni,Fe) phase, the Ni/Fe ratio determines the lattice parameter, as determined by Havinga and co-workers [18]. If chemistry were the only cause for lattice parameter changes, the best fit to our data would imply a Ni/Fe ratio of about 9 in the precipitates, whereas this ratio is commonly found to be near 1. However, as mentioned above, there are other reasons for these changes.

The analysis of the precipitate volume fraction from the X-ray data is complicated by the fact that there are different types of precipitates, and their relative proportions depend on non-equilibrium processes of alloying element partitioning between the second-phase and the matrix. We performed some additional analysis on the simplest case we had, that of Zircaloy-4, which has only one type of precipitate. We analyzed the X-ray pattern from a series of Zircaloy-4 measurements using the Rietveld method as implemented in the GSAS program [19,20]. The Rietveld Method creates a fit to the X-ray data by simultaneously varying several parameters, including crystal structure parameters, scattering factors, and equipment characteristics. The method fits the spectrum as a whole and, as such, it yields simultaneously all the pattern parameters, including as lattice parameters, volume fractions, texture, etc. We calculated the precipitate volume fraction at each CAP using this method.

For the Zircaloy-4 annealing experiment shown in Fig. 4, we calculated the precipitate volume fraction from the GSAS fit of the data. Figure 7 shows the precipitate volume fraction as a function of CAP, normalized to the measured precipitate volume fraction at CAP = 10⁻¹⁶ h calculated from the measurement. The normalization process factors out the lack of knowledge in the absolute value of the volume fraction introduced by unknown values of the GSAS parameters. Assuming total precipitation of the alloying elements and assuming the composition reported in Table 2, we calculate a volume fraction of 0.45% at 10⁻¹⁶ h (not considering any corrections to precipitates volume from misfit strains and/or defects such as stacking faults which may be present in the precipitates). The actual value of the volume fraction will be smaller than this, as some of the alloying elements will be dissolved in the matrix. The precipitate volume fraction increases with increasing annealing parameter, showing an S-shape. The data show that most of the precipitation occurs between 10⁻¹⁹ and 10⁻¹⁸ h.

We can also use the data to estimate the size of the precipitates from the line-broadening of the precipitate peaks associated with particle size. The particle size d is given by the Scherrer equation [21]:

$$d = \frac{0.9 \lambda}{B_{\theta} \cos \theta} \quad (2)$$

where $B_{\theta} = (B^2 - B_i^2)^{1/2}$ is the particle size broadening for peak θ , B is the measured peak broadening (full-width half maximum, FWHM), B_i is the instrumental broadening measured using a standard, θ is the diffraction angle, and λ is the wavelength of the synchrotron radiation. Using a pattern measured from a LaB₆ standard obtained from NIST, we determined the instrumental broadening in this case to be 0.039 two-theta. This technique for

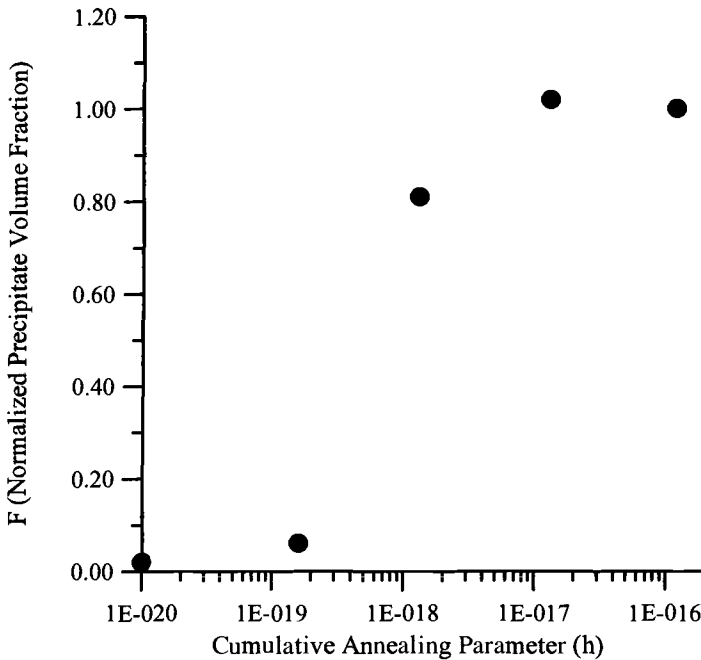


FIG. 7—Normalized precipitate volume fraction versus annealing parameter (CAP) for $Zr(Cr,Fe)_2$ precipitates in Zircaloy-4.

measuring particle size is useful in the range 0 to 100 nm, which coincidentally is the range of greater interest for the present experiments, as the precipitate size when fully annealed is on the order of 100 to 200 nm [3].

The Zr peaks show little broadening for CAP above 10^{-20} h, but the particle peaks clearly sharpen as the CAP increases. We calculated the particle sizes for the second phase peaks shown in Figs. 3 and 4 and which correspond to the isochronal anneals shown in Table 2, using the 200 and 112 peaks located at between 25 and 26° two-theta. The reason for this choice is that these peaks are reasonably isolated and because they are present in samples with CAP as low as 10^{-20} h. We determined the FWHM of the peaks by fitting the peak profiles using a Pearson VII-type curve shape (after subtracting background) using the program PeakFit 4.0 to determine the FWHM. These results show a degree of variability of 10% from one fit to the other. The particle-size results calculated using Eq 2 are plotted in Fig. 8 against the log of the CAP. The squares and circles represent two different runs performed on similar samples. It is clear that the $Zr(Cr,Fe)_2$ particle size in Zircaloy 4 increases continuously until 10^{-17} h, at which point the particle size saturates. The range of particle sizes calculated here corresponds reasonably well with the particle size seen in TEM examinations of these samples. As mentioned by Gros and Wadier [3], the particle size does not depend solely on the CAP. For a given CAP a longer anneal at lower temperature will produce slightly larger particles than a shorter anneal at high temperature. For the annealing conditions they used, in their TEM observations (reported only for CAP $> 10^{-17}$ h) their precipitate sizes were about 135 nm at 1.46×10^{-17} h and 150 nm at 1.07×10^{-16} h. In the present measurements, the corresponding calculated values are 90 and 120 nm, respectively. As mentioned in the introduction, it is difficult to obtain a good estimate of the

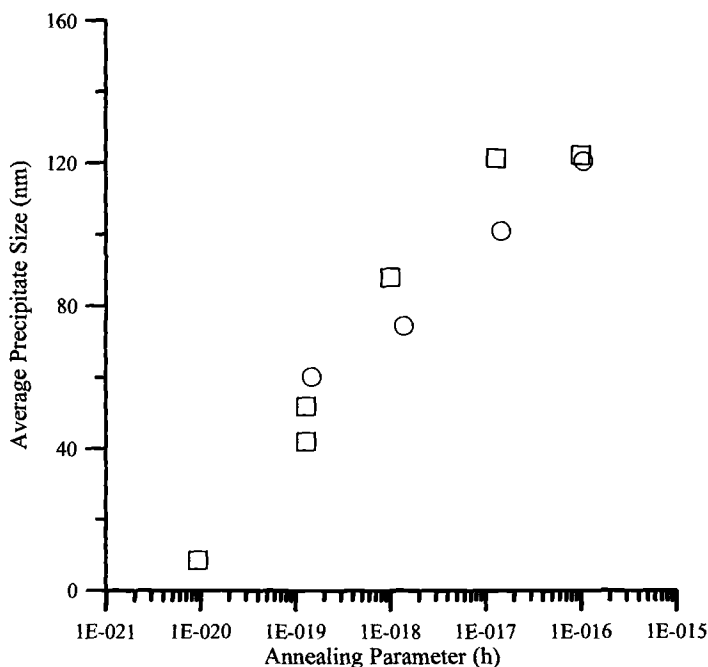


FIG. 8—Average $Zr(Cr,Fe)_2$ particle size in Zircaloy-4 versus annealing parameter as measured by diffraction line broadening. Circles and squares indicate two runs conducted on two similar but separate sets of samples.

precipitate size distribution using TEM because of the difficulty in getting good statistics and because of other biases inherent to TEM, such as the possibility of overlooking smaller size precipitates that do not happen to be in contrast, so that the lower end of precipitate size distribution is cut off, as can be seen in Ref 3. Thus it is possible that artificially large average precipitate sizes would be reported in TEM studies, because the small precipitates evade detection. However, the present method also has its limitations, especially at the higher precipitate sizes when the peak broadening starts to become comparable to the instrument broadening, so that precipitate size increases in the 100 to 200 nm may be difficult to detect. The present method gives, however, a window into the earlier times of precipitation from solution (10^{-20} to 10^{-19} h) when precipitate sizes are small. We should also note that the range of scatter observed in Fig. 8 is partly due to the variation inherent in different annealing schedules for a given CAP. In general, the higher precipitate sizes correspond to lower annealing temperatures.

Micro X-Ray Fluorescence

To analyze the fluorescence spectra, we used the MSIM5D program [22]. This Monte Carlo program simulates the interaction of an X-ray photon beam with a slab sample of arbitrary composition, explicitly taking into account all the scattering and fluorescence emission processes from both the material and from air. In performing the analysis, we entered our experimental conditions (sample composition, incident energy, geometry, acceptance angle, etc.) as input for the simulation (we used the detector efficiency provided by the man-

ufacturer to simulate the response of our EDS detector). We then compared the simulated spectrum with our experimental data and adjusted the input concentrations until the spectra matched. The concentrations that make the simulations agree with the measured spectra are our calculated concentrations. In this fitting procedure, spectra had to be normalized to account for unknown sample thickness: this was done by equating the simulated and experimental intensities obtained from an element of known concentration. Because the detector efficiency falls fairly sharply with energy in the region below 3 keV, we used the Sn L peaks to normalize the spectrum rather than using the Zr L peaks, i.e., for any given spectrum we normalized the data so that the curves agreed with experimental values in the Sn L region. The rest of the curve was fit by varying the concentration of the alloying elements with no other adjustable parameters. By performing this simulation on the standards (quenched alloys with a homogeneous distribution of alloying elements and equal to the bulk concentration), we can verify that the simulation and fitting procedure reproduce the known compositions. Figure 9a shows the measured and simulated spectra for quenched Zircaloy-4 and matrix of Zircaloy-4, and Fig. 9b shows the equivalent values for "ZIRLO." We note that because the alloys were annealed at very high CAP ($\sim 10^{-16}$ h), the ZIRLO alloy has only the composition but not the microstructure of ZIRLO. The values of the alloying element concentrations used to fit the spectra are shown in the legend. We note that the curve fit is very good for all the elements in the alloy. Even the Zr peak agrees well, despite the rapid variation of detector efficiency in its region. The agreement with the measured bulk concentrations shown in Table 1 is excellent.

We analyzed the fluorescence spectra obtained at a Zircaloy-4 matrix point such as shown in Fig. 5. The concentrations needed to fit the spectrum are Sn: 1640 wt ppm, Fe: 300 wt ppm, Cr: 270 wt ppm. We should note that the Cu level is higher than that measured in Table 1, but the interference of the elastic peak, and the very high fluorescence yield of Cu at these beam energies, make this measurement not as precise as the other elements. Measuring the level of Fe and other alloying elements in the matrix is one of the primary goals of this experiment, so we made concerted efforts to ensure that the measured alloying element concentrations are representative of the matrix. Thus, we used TEM samples to minimize the problem of hitting a "buried" precipitate, carefully locating the beam in a region away from the precipitate peaks and performing several measurements at different spots in the matrix region. The matrix concentrations of Fe and Cr above are on the order of measurements performed in Zircaloy-2 by Kruger et al. [23], who found a matrix value of ~ 140 wt ppm using atom probe, and of the results obtained by Wadman et al. [24], who found Fe concentrations in the Zircaloy-4 matrix between 110 and 190 wt ppm, but up to a factor of 2 higher. One of the possible reasons for the difference is that, in the present case, very small precipitates (< 80 nm) cannot be clearly distinguished from the matrix. If the current results are valid, this could mean that the actual concentration of alloying elements in the matrix is higher than the equilibrium concentration. These alloying elements may be in metastable equilibrium in the matrix, possibly associated with other alloying elements (such as O or Sn) and with lattice defects, such as dislocations and stacking faults.

Conclusions

We have performed detailed X-ray diffraction and X-ray microfluorescence measurements of various zirconium alloys using synchrotron radiation. The results should be considered preliminary and should be confirmed by more detailed analysis. The main results are as follows:

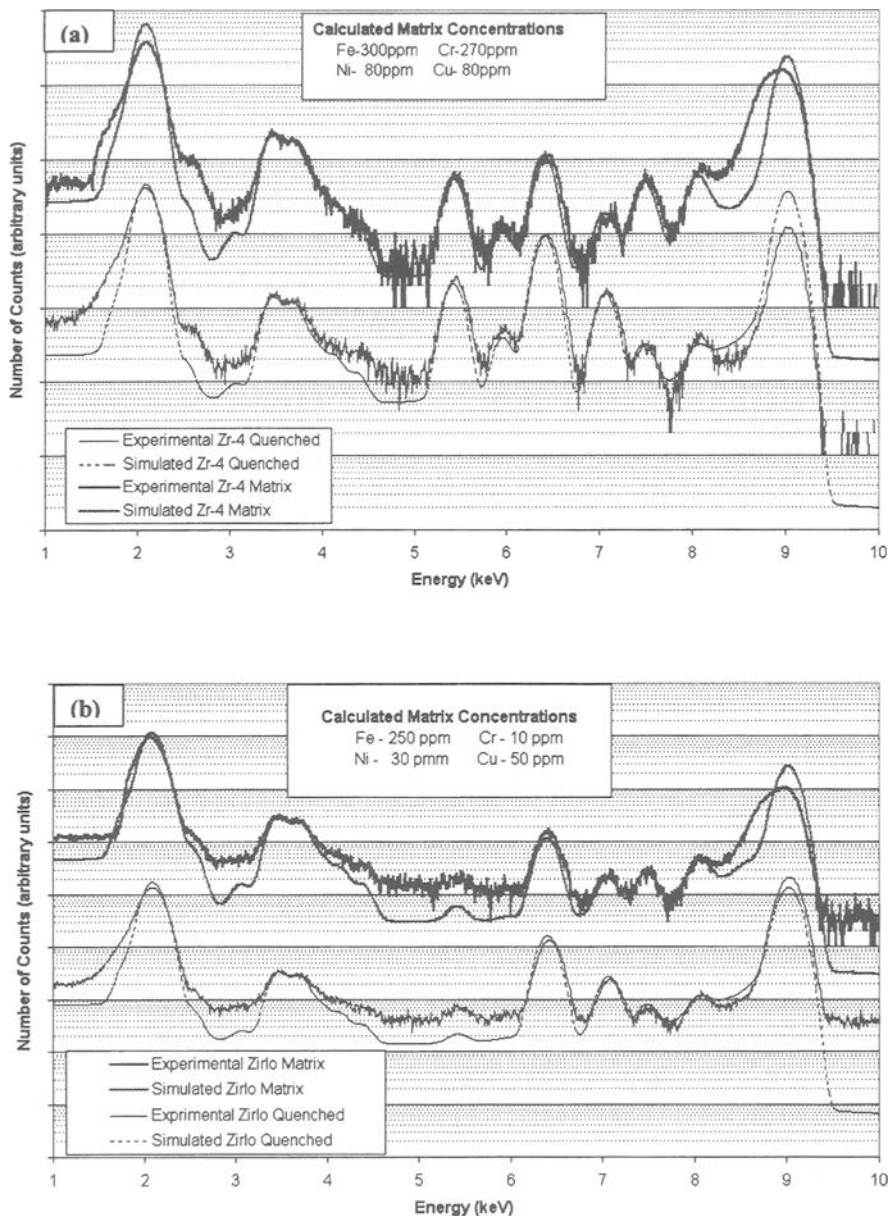


FIG. 9—(a) X-Ray intensity versus energy for quenched Zircaloy-4 and the matrix region of a fully recrystallized Zircaloy-4 ($CAP = 10^{-16}$ h) TEM sample (solid lines) and MSIM5D Monte Carlo simulations (dashed lines), using the concentrations shown in the figure. (b) X-ray intensity versus energy for quenched ZIRLO and the matrix region of a “ZIRLO” ($CAP = 10^{-16}$ h) TEM sample (solid lines) and MSIM5D Monte Carlo simulations (dashed lines), using the concentrations shown in the figure.

- The results presented here show that, using synchrotron radiation, it is possible to detect and quantify the very small volume fractions of second phase particles in the bulk alloy, which opens up the possibility of studying precipitate evolution in bulk irradiated material.
- We identified the second phase precipitates in bulk Zircaloy-4, Zircaloy-2, and ZIRLO, finding good agreement with literature values.
- We used synchrotron radiation to follow the precipitation kinetics in various zirconium alloys, as a function of annealing parameter. Most of the precipitation occurs between 10^{-19} and 10^{-18} h.
- The average $Zr(Cr,Fe)_2$ precipitate size in Zircaloy-4, as measured from the line broadening, increases from 10 nm at 10^{-20} h to 120 nm at 10^{-16} h.
- We performed measurements of the alloying element concentration in the matrix of Zr alloys, finding good agreement for the homogeneous alloys (quenched alloys, nominally pure and ultra pure Zr).
- The analysis of the spectra obtained from the matrix of Zircaloy-4 at 10^{-16} h indicate Fe matrix concentrations on the order of 300 ppm.

This work shows that synchrotron radiation is an extremely useful tool for obtaining detailed microstructural information of metallic alloys, in the bulk, and spatially resolved on a sub-micron scale. One of the significant consequences of this work is that it reveals a bulk characterization technique that can reveal detailed information about the microstructure of the alloy, which can be used for alloy optimization.

Acknowledgments

Thanks are due to Aylin Yilmazbayhan and Sarah Jurgensmeier for their help with data collection and for preparing some of the figures. The authors would like to thank R. B. Adamson at G. E. Vallecitos, L. M. Howe of AECL, Chalk River Laboratories, and R. J. Comstock and G. P. Sabol at Westinghouse Science and Technology Center for furnishing the samples used in this study. A. T. Motta would like to acknowledge helpful discussions with R. J. Comstock on synchrotron radiation that inspired this study, and with P. Heaney and R. Von Dreele on the use of GSAS. Thanks are also due to Laszlo Vincze for furnishing us with the copy of his program MSIM5D and for helping us set it up for our purposes.

Use of the Advanced Photon Source was supported by the U.S. Department of Energy, Basic Energy Sciences, Office of Science, under Contract No. W-31-109-Eng-38. This research was sponsored by the Department of Energy, Nuclear Engineering Education and Research (DOE-NEER) program, under grant number DE-FG07-98ID 13637.

References

- [1] Garzarolli, F. and Holzer, R., "Waterside Corrosion Performance of Light Water Power Reactor Fuel," *Journal of the British Nuclear Society*, Vol. 31, 1992, pp. 65–85.
- [2] Garzarolli, F. and Stehle, H., *IAEA Symposium on Improvements in Water Reactor Fuel Technology and Utilization*, Vol. SM 288/24, IAEA, 1986, pp. 387–407.
- [3] Gros, J. P. and Wadier, J. F., "Precipitate Growth Kinetics in Zircaloy-4," *Journal of Nuclear Materials*, Vol. 172, 1990, pp. 85–96.
- [4] deCarlan, Y., Regnard, C., Griffiths, M., Gilbon, D., and Lemaignan, C., "Influence of Iron in the Nucleation of $\langle c \rangle$ Component Dislocation Loops in Irradiated Zircaloy-4," *11th International Symposium on Zr in the Nuclear Industry, STP 1295*, ASTM, 1996, pp. 638–651.

- [5] IAEA, "Corrosion of Zirconium Alloys in Nuclear Power Plants," IAEA, Vienna IAEA-TECDOC-684, 1993.
- [6] Charquet, D. and Alheritiere, E., Workshop on Second-Phase Particles in Zircaloy, *F.R.G. Kerntechnische Gessellschaft*, 1985, pp. 5–11.
- [7] Zou, H., Hood, G. M., Roy, J. A., Packwood, R. A., and Weatherall, V., "Solute Distribution in Annealed Zircaloy-2 and Zr-2.5Nb," *Journal of Nuclear Materials*, Vol. 208, 1994, pp. 159–165.
- [8] Cai, Z., Lai, B., Yun, W., Ilinski, P., Legnini, D., Maser, J., and Rodrigues, W., "A Hard X-Ray Scanning Microprobe for Fluorescence Imaging and Microdiffraction at the Advanced Photon Source," *The Sixth International Conference for X-Ray Microscopy, AIP Proceedings*, Vol. 507, 2000, p. 472.
- [9] Yun, W., Lai, B., Cai, Z., Maser, J., Legnini, D., Gluskin, E., Chen, Z., Krasnoperova, A., Valdimirsky, Y., Cerrina, F., Fabrizio, E. D., and Gentili, M., "Nanometer Focusing of Hard X-Rays by Phase Zone Plates," *Review of Scientific Instruments*, Vol. 70, 1999, pp. 2238.
- [10] Sabol, G. P., Comstock, R. J., Weiner, R. A., Larouere, P., and Stanutz, R. N., "In-Reactor Corrosion Performance of ZIRLO and Zircaloy-4," *10th ASTM International Symposium on Zr in the Nuclear Industry, STP 1245*, ASTM, 1994, pp. 724–744.
- [11] Wang, J., Motta, A. T., and Comstock, R. J., "Crystal Structure of Intermetallic Precipitates in ZIRLO," to be submitted to the *Journal of Nuclear Materials*.
- [12] Sabol, G. P., Kilp, G. R., Balfour, M. G., and Roberts, E., "Development of a Cladding Alloy for High Burnup," *Eighth International Symposium on Zirconium in the Nuclear Industry, STP 1023*, ASTM, 1989, pp. 227–244.
- [13] International Center for Diffraction Data, Reference Card 42-1289, Newton, PA, 2001.
- [14] Erwin, K. T., Delaire, O., Motta, A. T., Birtcher, R. C., Chu, Y., and Mancini, D., "Observation of Second-Phase Particles in Bulk Zirconium Alloys Using Synchrotron Radiation," *Journal of Nuclear Materials*, Vol. 294, 2001, pp. 299–304.
- [15] International Center for Diffraction Data, Reference Card 38-1170, Newton, PA, 2001.
- [16] International Center for Diffraction Data, Reference Card 35-0789, Newton, PA, 2001.
- [17] International Center for Diffraction Data, Reference Card 5-065, Newton, PA, 2001.
- [18] Havinga, E. E., Damsma, H., and Hokkeling, P., "Compounds and Pseudo Binary Alloys with CuAl₂-C16-Type Structure, Pt.1: Preparation and X-Ray Results," *Journal of the Less-Common Metals*, Vol. 27, 1972, pp. 169–186.
- [19] Larson, A. C. and Von Dreele, R. B., "GSAS-General Structure Analysis System," LANL, Los Alamos LAUR 86-748, 1994.
- [20] Larson, A. C. and Von Dreele, R. B., "General Structure Analysis System (GSAS)," Los Alamos National Laboratory, Report LAUR 86-748, 2000.
- [21] Cullity, B. D., *Elements of X-ray Diffraction*, Addison-Wesley, Reading, MA, 1978.
- [22] Vincze, L., Janssens, K., Adams, F., and Jones, K. W., "A General Monte Carlo Simulation of Energy-Dispersive X-Ray Fluorescence Spectrometers—Part 3. Polarized Polychromatic Radiation, Homogeneous Samples," *Spectrochimica Acta, Part B*, Vol. 50, 1995, pp. 1481–1500.
- [23] Kruger, R. M., Adamson, R. B., and Brenner, S. S., *Journal of Nuclear Materials*, Vol. 189, 1992, pp. 193–200.
- [24] Wadman, B. and Andren, H.-O., "Microanalysis of the Matrix and the Oxide-Metal Interface of Uniformly Corroded Zircaloy," *Zirconium in the Nuclear Industry: Ninth international Symposium, STP 1132*, ASTM, 1991, pp. 461–475.

DISCUSSION

*R. K. Srivastava*¹ (*written discussion*)—Whether ZIRLO is being used as fuel tube material for any nuclear reactor?

A. T. Motta et al. (*authors' closure*)—ZIRLO is currently being used in many light water reactors all over the world as nuclear fuel cladding.

*N. Ramasubramanian*² (*written discussion*)—For an annealing parameter there is a distribution in size of precipitates. Does the synchrotron signal indicate the presence of a multiplicity of peaks for the size distribution of precipitates?

A. T. Motta et al. (*authors' closure*)—The only indication the synchrotron signal gives of precipitate size is in the line broadening associated with the diffraction peaks of the second phase particles, such as shown in Fig. 8. The information from many different precipitate sizes is convoluted in the signal and can be related to an average precipitate size according to the Scherrer equation (Eq 2 in our paper), thus we have information only on the average size.

*Elisabeth Ahlberg*³ (*written discussion*)—What is the detection limit with regards to size in your X-ray diffraction measurement? Small particles are X-ray amorphous and as you anneal the sample more particles will be visible in the X-ray diffraction pattern. Did you take this into account in your analysis of precipitation kinetics?

A. T. Motta et al. (*authors' closure*)—Because we are studying the crystalline X-ray diffraction peaks, we can only study the precipitates that scatter X-rays coherently. Since we were not aware of any references that indicated that small precipitates in Zircalloys are X-ray amorphous, we equated the crystalline volume fraction with the precipitate volume fraction. If, as you indicate, small particles are X-ray amorphous, then we would not detect these particles.

*Heinz Ruhmann*⁴ (*written discussion*)—You reported about 300 ppm Fe to be found in the matrix. Does this mean that the matrix is supersaturated and not in equilibrium? Are there indications of Fe deposition?

A. T. Motta et al. (*authors' closure*)—We presume that by iron deposition you mean during the electro-polishing process; we were also concerned about this effect and performed additional experiments that indicate that this effect is not important. Briefly, we examined an electropolished sample in the as-prepared state and after a few minutes of ion milling and found there was no change in the Fe content in the matrix. If such Fe deposition had occurred, the ion milling would have removed the surface layer and led to a lower measured concentration in the ion milled sample.

Concerning the high Fe concentration, we believe that there are two explanations: (i) that the alloying elements are not in “equilibrium” in the matrix, and (ii) that the equilibrium solid solubility for Fe in the Zircaloy (containing matrix defects and other alloying elements that can hold the Fe in solution) occurs at a higher alloying content than that measured in pure Zr (i.e., the thermodynamic solid solubility of Fe in Zr is altered by the other alloying elements and possibly by the lattice defects).

¹ N.F.C. Hyderabad, India.

² ECCATEC Inc.

³ Goteborg University.

⁴ Framatome ANP.

*Pierre Barberis*⁵ (*written discussion*)—Did you analyze the chemical composition of the second phase particles and its evolution with CAP? Did you compute the balance between the alloying elements in the matrix and that in the SPP?

A. T. Motta et al. (*authors' closure*)—We did not analyze the chemical composition of the second phase particles, and did not perform an elemental balance, although this could be an interesting exercise to perform. This is because we only measured alloying element content in the matrix in the quenched state and at CAP = 10⁻¹⁶ h, and because our results for precipitate volume fraction are only semi-quantitative at this point. Once we have a more quantitative value for the volume fraction of second-phase particles, we can infer how much of the Fe is tied up in precipitates and how much is in the matrix.

*Brian Cox*⁶ (*written discussion*)—1. I noticed values of 50–80 ppm of Cu in your X-ray fluorescence data. Was this present in the specimen holder?

2. Have you calculated the energy deposition density in the synchrotron experiments and is it so high that you could not use this technique for an insulating specimen such as an oxide film?

A. T. Motta et al. (*authors' closure*)—You raise a good point. The chemical analysis performed independently shows an impurity level of Cu of about 20 wt ppm in the alloy. For the energies we use in the synchrotron, Cu scatters very efficiently, and very small changes in detector efficiency or in the elastic peak could yield a factor of two in the Cu concentration. The concentrations of Cu reported here are probably not reliable for that reason, but since we were not interested in pinning down the exact Cu concentration, we did not make that value more precise. We have included a sentence to that effect in the text.

Although we have not calculated the beam heating, there are no signs that it is excessive or that the temperature of the samples is too high during the experiment (no sample discoloration, etc.). We have been examining zirconium alloy oxides in the synchrotron and found no evidence of temperature rise in those samples either.

*Jean-Christophe Brachet*⁷ (*written discussion*)—We have made some in-situ neutron diffraction experiments on Zr-Nb-Fe alloys (see paper of Toffolon et al.) we have observed that upon heating from 20°C to 580°C, the diffraction peaks of SPP (Zr-Nb-Fe) sharpen. We have made the assumption that it was partially due to relaxation of internal stress due to the difference of thermal expansion coefficients between SPP and the matrix.

Did you take into account this phenomenon to interpret the broadening/sharpening of your SPP diffraction peaks?

A. T. Motta et al. (*authors' closure*)—All our measurements were made at room temperature, and thus result from microstructural changes induced by the annealing rather than the physical phenomena you describe. As mentioned in the text such stress-induced broadening caused by stresses originating from the cooling process may also be present in our samples, but we have not evaluated its extent. In any case, since all of our observations are performed at room temperature, the sharpening we observe in the current work as CAP increases is clearly due to the changes induced by the annealing.

⁵ Framatome.

⁶ University of Toronto.

⁷ CEA.